Illustration of universal relations for trapped four-fermion system with arbitrary s-wave scattering length

D. Blume[1] and K. M. Daily[1]

[1]*Department of Physics and Astronomy, Washington State University, Pullman, Washington 99164-2814, USA*
(Dated: September 15, 2009)

A two-component four-fermion system with equal masses, interspecies s-wave scattering length a_s and vanishing intraspecies interactions under external spherically symmetric harmonic confinement is considered. Using a correlated Gaussian basis set expansion approach, we determine the energies and various structural properties of the energetically lowest-lying gas-like state throughout the crossover for various ranges of the underlying two-body potential. Extrapolating to the zero-range limit, our numerical results show explicitly that the total energy, the trap energy as well as certain aspects of the pair distribution function and of the momentum distribution are related through the so-called integrated contact intensity $I(a_s)$. Furthermore, it is shown explicitly that the total energy and the trap energy are related through a generalized virial theorem that accounts for a non-zero range.

PACS numbers:

I. INTRODUCTION

Dilute equal-mass two-component Fermi gases at unitarity, i.e., gases with infinitely large interspecies s-wave scattering length a_s and vanishing intraspecies scattering length, show unique universal properties [1, 2, 3, 4, 5, 6, 7, 8, 9]. Here, the term dilute means that nr_0^3 is much smaller than 1, where r_0 denotes the range of the underlying two-body potential and n the density of the system (for trapped gases, n stands for the peak density). Intuitively, the existence of universal properties of the unitary two-component Fermi gas can be understood by realizing that the infinitely large s-wave scattering length a_s does not establish a meaningful length scale for the system. Correspondingly, the only length scale of the infinitely strongly interacting system is set by the density (for homogeneous systems) or the trapping potential (for inhomogeneous systems). The fact that the unitary two-component Fermi gas is characterized by a single length scale makes it, in certain respects, similar to the non-interacting system. The above argument has been formalized within a hyperspherical framework [8]. It has been shown, e.g., that the harmonically trapped two-component Fermi gas is characterized, just as the non-interacting system, by ladders of states whose energies are spaced by $2\hbar\omega$ [8, 10], where ω denotes the angular trapping frequency. The $2\hbar\omega$ spacing has been verified semi-analytically for the trapped two- and three-fermion systems [11, 12] and numerically for systems with up to six fermions [13]. In addition, a number of other universal relations have been established at unitarity [1, 2, 3, 4, 5, 6, 7, 8, 9].

More recently, the notion of universal relations has been extended to dilute equal-mass two-component Fermi gases with finite interspecies scattering length a_s for which the two-body range r_0 is small compared to a_s [14, 15, 16, 17, 18, 19]. While it has been established early on that the behaviors of these systems through the crossover is governed by the s-wave scattering length a_s

alone (see Ref. [20] for a review) and that the system is, in this sense, universal, only recently has there been significant progress in relating seemingly disconnected quantities such as the total energy, the expectation value of the trapping potential, the pair distribution function and the momentum distribution through universal relations that involve a quantity termed the integrated contact intensity $I(a_s)$ [14, 15, 16]. Physically, the integrated contact intensity measures the "number of pairs per unit length". It vanishes for vanishing a_s, indicating the absence of pairs, and increases as the system enters the strongly-interacting and eventually the weakly repulsively-interacting BEC regime, where the pairs turn into actual molecules [21, 22].

This paper explicitly tests, to the best of our knowledge for the first time, the equivalence of four definitions of the integrated contact intensity $I(a_s)$ [14, 15, 16]. In doing so, we explicitly determine the integrated contact intensity for the energetically lowest-lying gas-like state of the four-fermion system. The spin-balanced four-fermion system possesses non-trivial correlations and can, at least in principle, be realized by loading a degenerate Fermi gas consisting of dimers into an optical lattice (see, e.g., Ref. [23]). Once a situation with one molecule per site is realized, neighboring sites can be merged and molecules dissociated by changing the s-wave scattering length. This scheme would allow for the realization of an array of four-fermion systems with adjustable s-wave scattering length a_s. The integrated contact intensity determined in Sec. III, combined with the imaginary part of the two-body s-wave scattering [18], readily leads to a prediction of the atom losses due to inelastic two-body collisions, an experimentally observable quantity. Our results thus provide not only an illustration of the equivalence of various definitions of $I(a_s)$ but also pave the way for making quantitative predictions.

Section II reviews the definition of the integrated contact intensity $I(a_s)$ for a trapped two-component Fermi gas interacting through a zero-range potential with s-

wave scattering length a_s. Section III illustrates the equivalence of various definitions of the integrated contact intensity numerically. To this end, we solve the Schrödinger equation for the four-fermion system as a function of the range of the two-body potential and extrapolate our solutions to the zero-range limit. Section IV applies the generalized virial theorem derived by Werner [17] to our finite-range four-body energies. Lastly, Sec. V concludes.

II. DEFINITION OF THE INTEGRATED CONTACT INTENSITY

This section reviews the definitions of the integrated contact intensity $I(a_s)$ introduced by Tan [14, 15, 16]. For concreteness, we consider a two-component equal-mass Fermi gas consisting of N atoms under external spherically symmetric harmonic confinement in which unlike fermions interact through a short-range two-body potential V_{tb}. For this system, the model Hamiltonian H can be written as

$$H = \sum_{j=1}^{N} \left[-\frac{\hbar^2}{2m}\nabla_j^2 + \frac{1}{2}m\omega^2 \vec{r}_j^2 \right] + \sum_{j=1}^{N_\uparrow}\sum_{k=1}^{N_\downarrow} V_{\text{tb}}(r_{jk}), \quad (1)$$

where m denotes the atom mass, ω the angular trapping frequency, $N_\uparrow$ the number of spin-up atoms, $N_\downarrow$ the number of spin-down atoms, and $\vec{r}_j$ the position vector of the jth atom measured with respect to the center of the trap. The spherically symmetric two-body potential V_{tb} depends on the interparticle distance r_{jk}, where $r_{jk} = |\vec{r}_j - \vec{r}_k|$. Throughout, we assume that V_{tb} is characterized by two length scales, the s-wave scattering length a_s and the range r_0; this assumption implies, e.g., that the p-wave scattering length and other higher partial wave scattering lengths are zero. The lengths a_s and r_0, together with the harmonic oscillator length a_{ho}, where $a_{\text{ho}} = \sqrt{\hbar/(m\omega)}$, constitute the relevant length scales of the Hamiltonian H. Section III discusses our solutions to the stationary Schrödinger equation $H\psi = E\psi$, where the many-body wave function ψ depends on the coordinates of all particles, i.e., $\psi = \psi(\vec{r}_1, \cdots, \vec{r}_N)$. Throughout, we indicate the dependence of the eigenenergy E on the s-wave scattering length a_s and the range r_0 of the underlying two-body potential explicitly, i.e., we write $E = E(a_s, r_0)$.

The integrated contact intensity $I(a_s)$ introduced by Tan [14, 15, 16] applies to the Hamiltonian given in Eq. (1) in the limit that the two-body potential V_{tb} is characterized by a vanishing range r_0. Although the zero-range limit is, strictly speaking, not realized in nature, cold atom systems come arbitrarily close: The range of the two-body potential between two alkali atoms is set by the van der Waals tail, which—to leading order—falls off as C_6/r_{jk}^6; typical values of the van der Waals length for alkali atoms are of the order of $100a_0$ [24]. The zero-range limit is thus approximately realized if the absolute value of the s-wave scattering length a_s and the harmonic oscillator length a_{ho} are much larger than the van der Waals length. This scenario can be realized in cold atom experiments by choosing a sufficiently small trapping frequency ω and by tuning the s-wave scattering length through the application of an external magnetic field in the vicinity of a Fano-Feshbach resonance. In the zero-range limit, the two-body interactions impose the Bethe-Peierls boundary condition whenever two unlike particles approach each other (see, e.g., Ref. [20]), making even the strongly-correlated many-body problem amenable to analytical treatments.

The integrated contact intensity $I(a_s)$ can be defined through four distinct relationships [see (i) through (iv) below] [14, 15, 16]; as such, the integrated contact intensity establishes non-trivial connections between properties such as the energy, the pair distribution function and the momentum distribution of the two-component Fermi gas with zero-range interactions. For concreteness, we restrict ourselves to the zero temperature situation, where expectation values are calculated for a given many-body eigenstate $\psi(\vec{r}_1, \cdots, \vec{r}_N)$. We note, however, that the Tan relations can be generalized to finite temperature [14].

(i) The *adiabatic energy relation* [14, 15, 16] defines the integrated contact intensity $I(a_s)$ through

$$I_{\text{adia}}(a_s) = \frac{4\pi m}{\hbar^2}\frac{\partial E(a_s, 0)}{\partial\left(-a_s^{-1}\right)}. \quad (2)$$

(ii) The *virial relation* [14, 15, 16] defines the integrated contact intensity $I(a_s)$ through

$$I_{\text{virial}}(a_s) = \frac{8\pi m a_s}{\hbar^2}\left[2V_{\text{tr}}(a_s, 0) - E(a_s, 0)\right], \quad (3)$$

where $V_{\text{tr}}(a_s, r_0)$ denotes the expectation value of the trapping potential, $V_{\text{tr}} = \langle \sum_j m\omega^2 r_j^2/2 \rangle$. We refer to V_{tr} as trap energy.

(iii) The *pair relation* [14, 15, 16] defines the integrated contact intensity in terms of the number $N_{\text{pair}}^{r<s}$ of up-down pairs with distances r smaller than s,

$$I_{\text{pair}}(a_s) = \lim_{s\to 0}\frac{4\pi N_{\text{pair}}^{r<s}}{s}. \quad (4)$$

If $P_{\text{pair}}(r)$ denotes the pair distribution function for the up-down distance r, normalized such that

$$4\pi\int_0^\infty P_{\text{pair}}(r)r^2 dr = N_\uparrow N_\downarrow, \quad (5)$$

then Eq. (4) can alternatively be expressed as

$$I_{\text{pair}}(a_s) = \lim_{r\to 0}(4\pi)^2 P_{\text{pair}}(r) r^2, \quad (6)$$

where $P_{\text{pair}}(r)$ is understood to be calculated for zero-range interactions.

(iv) The *momentum relation* [14, 15, 16] defines the integrated contact intensity in terms of the number $N_{\text{atom}}^{k>K}$ of atoms with momentum k greater than K,

$$I_k(a_s) = \lim_{K \to \infty} \pi^2 \, K \, N_{\text{atom}}^{k>K}. \qquad (7)$$

This momentum relation can be reexpressed in terms of the momentum distribution $n_\uparrow(\vec{k})$ of the up-atoms and in terms of the momentum distribution $n_\downarrow(\vec{k})$ of the down atoms:

(iva) If $n_\uparrow(\vec{k})$ is normalized such that

$$\int n_\uparrow(\vec{k})d^3\vec{k} = N_\uparrow, \qquad (8)$$

then Eq. (7) can alternatively be expressed as

$$I_{k,\uparrow}(a_s) = \lim_{k^{-1} \to 0} 2\pi^2 \, 4\pi \, \frac{n_{00,\uparrow}(k)}{\sqrt{4\pi}} \, k^4, \qquad (9)$$

where $n_{00,\uparrow}(k)$ is defined through the partial wave expansion

$$n_\uparrow(\vec{k}) = \sum_{lm} n_{lm,\uparrow}(k)Y_{lm}(\hat{k}) \qquad (10)$$

and where $n_\uparrow(\vec{k})$ is understood to be calculated for zero-range interactions. The partial wave decomposition of $n_\uparrow(\vec{k})$ has been introduced to emphasize that $I_{k,\uparrow}(a_s)$ only depends on the spherically symmetric component of $n_\uparrow(\vec{k})$, i.e., only on k and not on $\vec{k}$.

(ivb) Alternatively, Eq. (7) can be rewritten in terms of the momentum distribution $n_\downarrow(\vec{k})$ of the down-atoms. To this end, the subscript "$\uparrow$" in (iva) needs to replaced by "$\downarrow$".

For $N_\uparrow = N_\downarrow$, we have $n_\uparrow(\vec{k}) = n_\downarrow(\vec{k}) = n(\vec{k})$ and $n_{00,\uparrow}(k) = n_{00,\downarrow}(k) = n_{00}(k)$, and consequently $I_{k,\uparrow}(a_s) = I_{k,\downarrow}(a_s) = I_k(a_s)$. For spin-imbalanced two-component Fermi gases, in contrast, relations (iva) and (ivb) establish a non-trivial relationship between the momentum distributions of the up- and down-atoms.

The quantities I_{adia}, I_{virial}, I_{pair}, $I_{k,\uparrow}$ and $I_{k,\downarrow}$ have been predicted to be identical [14, 15]. To the best of our knowledge this has, however, not yet been illustrated explicitly. In fact, the determination of the integrated contact intensity has so far only been pursued for a few selected systems and limiting cases [14, 15, 16, 18, 19]. Section III presents explicit calculations for the energetically lowest-lying gas-like state of the four-body fermion system throughout the crossover and numerically verifies the equivalence of the definitions (i) through (iv).

III. INTEGRATED CONTACT INTENSITY FOR FOUR-FERMION SYSTEM

This section determines the integrated contact intensity $I(a_s)$ for the energetically lowest-lying gas-like state

of the trapped four-fermion system with $N_\uparrow = N_\downarrow = 2$ as a function of the s-wave scattering length a_s according to definitions (i) through (iv). Unlike for the three-fermion problem (see, e.g., Ref. [25]), no analytical solutions are known for the four-fermion problem with zero-range interactions. Here, we solve the stationary Schrödinger equation for the four-fermion system numerically using the correlated Gaussian (CG) approach [13, 26, 27, 28, 29].

The CG approach[13, 26, 27, 28, 29] expands the wave function in terms of Gaussian basis functions Φ_l,

$$\psi(\vec{r}_1, \cdots, \vec{r}_N) = \sum_{l=1}^{B} c_l \left[\mathcal{A}\Phi_l(r_{12}, \cdots, r_{N-1,N}) \right], \quad (11)$$

where the c_k denote expansion coefficients and

$$\Phi_l(r_{12}, \cdots, r_{N-1,N}) = \exp\left(-\sum_{j<k}^{N} \frac{r_{jk}^2}{2d_{l,jk}^2} \right). \qquad (12)$$

Each basis function Φ_l is parameterized by $N(N-1)/2$ widths $d_{l,jk}$ (one for each interparticle distance), which are optimized semi-stochastically following the ideas outlined in Ref. [26]. In Eq. (11), B denotes the number of unsymmetrized basis functions. For the four-fermion system with two up- and two down-atoms, the antisymmerization operator $\mathcal{A}$ can be conveniently written in terms of the permutation operator P_{jk}, which exchanges the position vectors of the jth and kth atom. If the position vectors $\vec{r}_1$ and $\vec{r}_2$ belong to the up-atoms and the position vectors $\vec{r}_3$ and $\vec{r}_4$ to the down-atoms, then $\mathcal{A}$ can be written as

$$\mathcal{A} = 1 - P_{12} - P_{34} + P_{12}P_{34}. \qquad (13)$$

The basis functions Φ_l have vanishing total angular momentum L and positive parity π and are thus well suited to describe the energetically lowest-lying gas-like state of the four-fermion system which has $L^\pi = 0^+$ symmetry [13, 28, 29].

We parametrize the two-body potential between each pair of up-down atoms by a simple Gaussian potential with range r_0 and depth V_0,

$$V_{\text{tb}}(r) = -V_0 \exp\left(-\frac{r^2}{2r_0^2} \right). \qquad (14)$$

For this interaction potential, the Hamiltonian matrix elements can be calculated analytically [26]. Throughout, we restrict ourselves to two-body potentials that support either no or one s-wave two-body bound state in free-space. For a given range r_0, the depth V_0 ($V_0 \geq 0$) is adjusted so that the scattering length a_s takes the desired value. While V_{tb} leads, in general, to non-vanishing higer partial wave scattering lengths for finite r_0, the importance of these higher partial wave contributions decreases with decreasing r_0 and vanishes for $r_0 = 0$. To mimic the zero-range limit, we perform calculations for various

r_0 while keeping the s-wave scattering length fixed and extrapolate the quantity of interest to $r_0 = 0$ (see below). For the parameter combinations considered in this paper, we find that the ground state of the four-fermion system has gas-like character, i.e., that self-bound trimer and tetramer states are absent, in agreement with findings for zero-range interactions [30, 31].

The CG approach results in an upper bound to the exact ground state energy. Our calculations reported below employ between $B = 450$ and 500 basis functions; we have checked that larger basis sets do not lead to a significant reduction of the energy. Once the expansion coefficients c_l $(l = 1, \cdots, B)$ have been determined by diagonalizing the generalized eigenvalue problem (the linear dependence of the basis functions gives rise to a non-diagonal overlap matrix), we calculate other expectation values such as $V_{\mathrm{tr}}(a_s, r_0)$, $P_{\mathrm{pair}}(r)$ and $n_{00}(k)$. The matrix elements associated with these observables can be determined analytically and are readily implemented. The computational time for the determination of the ground state energy and the structural properties for a given a_s and r_0 amounts to about an hour on a single processor of a state of the art desktop computer.

Our calculations cover the weakly-attractive and weakly-repulsive regimes as well as the strongly-interacting unitary regime; in particular, we consider 41 scattering lengths in the interval $a_{\mathrm{ho}}/a_s \in [-10, 10]$. For negative scattering lengths a_s, we find that both the total energy $E(a_s, r_0)$ and the trap energy $V_{\mathrm{tr}}(a_s, r_0)$ vary linearly with r_0 for fixed a_s. For negative a_s, we typically consider three different ranges r_0, i.e., $r_0 = 0.01, 0.03$ and $0.05a_{\mathrm{ho}}$, and determine the zero-range quantities $E(a_s, 0)$ and $V_{\mathrm{tr}}(a_s, 0)$ by performing a linear two-parameter fit. We checked for selected scattering lengths that the inclusion of additional ranges leaves the fitting parameters essentially unchanged. As the inverse scattering length a_s^{-1} is increased to positive values, the total energy starts depending non-linearly on the range r_0. In this regime, we consider six different ranges r_0 $(r_0 \leq 0.03a_{\mathrm{ho}})$ for each a_s and determine the zero-range limit $E(a_s, 0)$ by performing a quadratic three-parameter fit. We find that a three-parameter fit provides a reliable description of the trap energy $V_{\mathrm{tr}}(a_s, r_0)$ for $a_{\mathrm{ho}}/a_s = 0$ to 2. For larger inverse scattering lengths, $V_{\mathrm{tr}}(a_s, r_0)$ is significantly smaller than the absolute value of the total energy and has thus a comparatively large uncertainty. For $a_{\mathrm{ho}}/a_s > 2$, we determine the zero-range limit of $V_{\mathrm{tr}}(a_s, r_0)$ by performing a linear two-parameter fit. While $V_{\mathrm{tr}}(a_s, r_0)$ may depend non-linearly on r_0 in this regime, our CG data do not allow for a reliable determination of the functional dependence.

As an example, circles and squares in Fig. 1(a) show $E(a_s, r_0)$ and $2V_{\mathrm{tr}}(a_s, r_0)$ in units of the oscillator energy E_{ho}, $E_{\mathrm{ho}} = \hbar\omega$, obtained by the CG approach as a function of the range r_0 at unitarity. Figure 1(a) shows that the CG quantities are well described by a linear fit (solid lines). Furthermore, the four-body results shown in Fig. 1(a) demonstrate the validity of the virial theo-
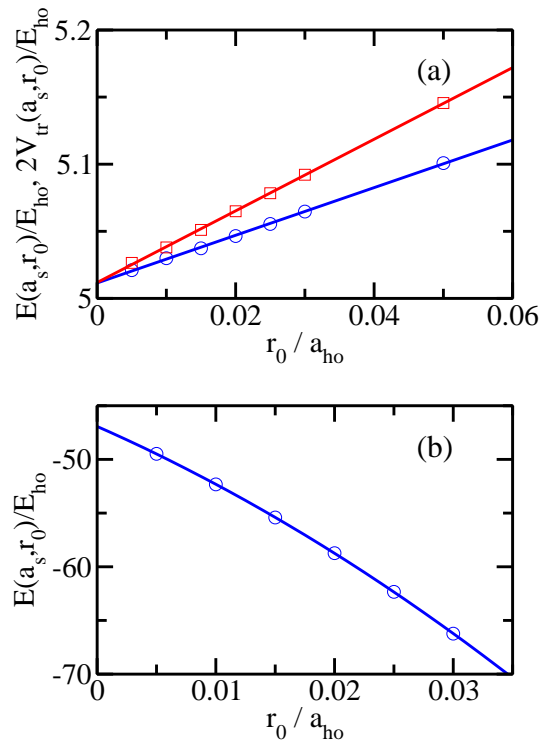

FIG. 1: (Color online) (a) Circles and squares show $E(a_s, r_0)$ and $2V_{\mathrm{tr}}(a_s, r_0)$, calculated using the CG approach, as a function of the range r_0 of the two-body interaction potential at unitarity, i.e., for $a_{\mathrm{ho}}/a_s = 0$. Solid lines show linear fits to the CG data. (b) Circles show $E(a_s, r_0)$, calculated using the CG approach, as a function of r_0 for $a_{\mathrm{ho}}/a_s = 5$. The solid line shows a quadratic fit to the CG energies. For both panels, the basis set error of the CG data is estimated to be smaller than the symbol size.

rem for zero-range interactions at unitarity [7, 8, 32, 33], which states that the energy equals twice the trap energy. We find that the linear fit to $E(\infty, r_0)$ and $2V_{\mathrm{tr}}(\infty, r_0)$, which includes all seven data points shown in Fig. 1(a), predicts the same intercepts within errorbars. In particular, we find $E(\infty, 0) = 5.0115(5)\hbar\omega$ and $2V_{\mathrm{tr}}(\infty, 0) = 5.0118(6)\hbar\omega$, where the number in round brackets indicates the uncertainty that results from the fit alone (excluding possible basis set errors of E and V_{tr} themselves). Our energy $E(\infty, 0)$ is slightly higher than the value of $5.0096\hbar\omega$ of Ref. [34]; this slight difference can be attributed to a tiny basis set error.

To illustrate the comparatively strong dependence of $E(a_s, r_0)$ on r_0 for positive scattering lengths, Fig. 1(b) shows the total energy as a function of r_0 for $a_{\mathrm{ho}}/a_s = 5$. In this case, the three-parameter fit results in a zero-range energy $E(a_s = a_{\mathrm{ho}}/5, 0)$ of $-46.93(3)\hbar\omega$, where the number in round brackets indicates the uncertainty that results from the fit alone (excluding possible ba-

sis set errors of the energies themselves). This uncertainty is larger than the uncertainty of $V_{\mathrm{tr}}(a_s, 0)$; in particular, we find $V_{\mathrm{tr}}(a_s = a_{\mathrm{ho}}/5, 0) = 1.619(2)\hbar\omega$. Even though the basis set extrapolation error associated with $V_{\mathrm{tr}}(a_s, r_0)$ might be somewhat larger than that associated with $E(a_s, r_0)$, our analysis suggests that the main uncertainty of the integrated contact intensities $I_{\mathrm{adia}}(a_s)$ and $I_{\mathrm{virial}}(a_s)$ in the small positive scattering length regime originates in the difficulty of determining the zero-range limit of $E(a_s, r_0)$ more reliably.

The extrapolated zero-range quantities $E(a_s, 0)$ and $V_{\mathrm{tr}}(a_s, 0)$ determine the integrated contact intensities $I_{\mathrm{adia}}(a_s)$ and $I_{\mathrm{virial}}(a_s)$ [see definitions (i) and (ii) above]. To determine $I_{\mathrm{adia}}(a_s)$, we interpolate $E(a_s, 0)$ and calculate its derivative with respect to a_s^{-1} based on this interpolation. Solid lines in Figs. 2(a)-2(c) show the integrated contact intensity $I_{\mathrm{adia}}(a_s)$ as a function of the inverse scattering length a_s^{-1}. Figure 2 shows that $I_{\mathrm{adia}}(a_s)$ increases monotonically with increasing a_s^{-1}. This monotonic increase reflects the increase of the two-body attraction with increasing a_s^{-1}. In going from the weakly-attractive regime ($a_{\mathrm{ho}}/a_s \leq -10$) to the weakly-repulsive regime ($a_{\mathrm{ho}}/a_s \geq 10$), the integrated contact intensity changes by about three orders of magnitude. For comparison, dotted lines show the integrated contact intensity $I_{\mathrm{virial}}(a_s)$. The two contact intensities $I_{\mathrm{adia}}(a_s)$ and $I_{\mathrm{virial}}(a_s)$ are nearly indistinguishable on the scales shown in Figs. 2(a)-2(c), thereby lending strong support for the equivalence of definitions (i) and (ii).

To quantify the agreement of $I_{\mathrm{adia}}(a_s)$ and $I_{\mathrm{virial}}(a_s)$, Fig. 3 shows the fractional difference between these two quantities. Figure 3 shows that the fractional difference is very small (less than 0.004) for negative scattering lengths where our extrapolated zero-range quantities $E(a_s, 0)$ and $V_{\mathrm{tr}}(a_s, 0)$ have the smallest uncertainties. For positive scattering lengths, the fractional difference shows a fairly systematic deviation from zero that might be attributed to small systematic errors of $E(a_s, 0)$ and $V_{\mathrm{tr}}(a_s, 0)$. The better than 1% agreement between $I_{\mathrm{adia}}(a_s)$ and $I_{\mathrm{virial}}(a_s)$ over the entire scattering length range considered lends strong numerical support for the prediction that Eqs. (2) and (3) constitute equivalent definitions of the integrated contact intensity $I(a_s)$.

Next, we discuss the determination of the integrated contact intensity from the pair distribution functions $P_{\mathrm{pair}}(r)$ for the up-down distance. Figure 4 shows exemplary scaled pair distribution functions for $r_0 = 0.005a_{\mathrm{ho}}$ and various s-wave scattering lengths a_s (see also Ref. [29]). In particular, Fig. 4(a) shows $(4\pi)^2 P_{\mathrm{pair}}(r)r^2$ for negative a_s while Figs. 4(b) and 4(c) show respectively the small r and the large r regions of $(4\pi)^2 P_{\mathrm{pair}}(r)r^2$ for positive a_s. The overall behavior of the pair distribution functions can be described as follows: (i) The amplitude at large r decreases with increasing a_s^{-1}, reflecting the fact that the four-fermion system becomes more compact with increasing attraction. (ii) As a_s^{-1} increases from $-10a_{\mathrm{ho}}^{-1}$ to 0 (and to even larger values), the scaled pair distribution functions develop a two peak structure that
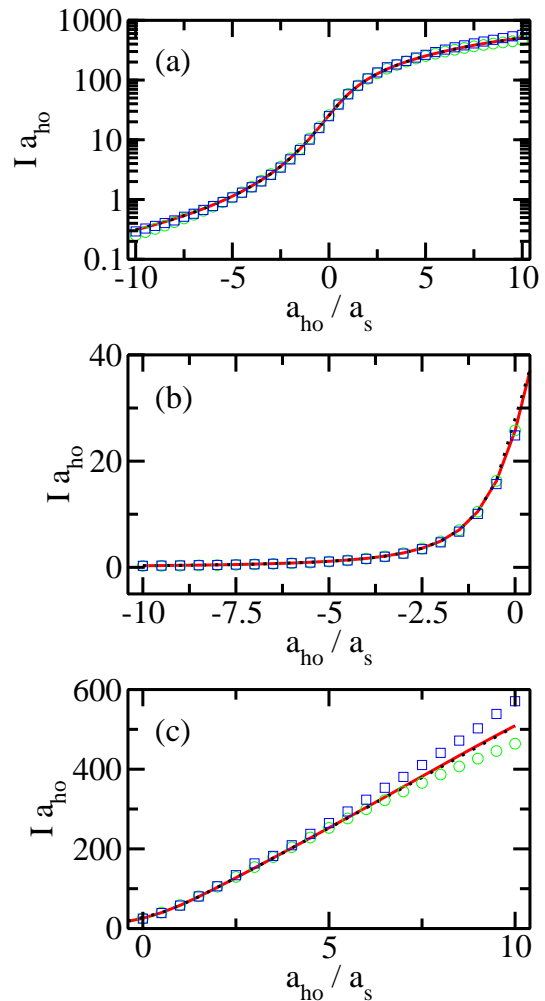

FIG. 2: (Color online) Integrated contact intensities $I_{\mathrm{adia}}(a_s)$, $I_{\mathrm{virial}}(a_s)$, $I_{\mathrm{pair}}(a_s)$ and $I_k(a_s)$ as a function of the inverse s-wave scattering length a_s^{-1}. Solid and dotted lines show the integrated contact intensities $I_{\mathrm{adia}}(a_s)$ and $I_{\mathrm{virial}}(a_s)$ calculated according to Eqs. (2) and (3), respectively, using the extrapolated zero-range quantities as input (the two data sets are nearly indistinguishable on the scale shown and compared in more detail in Fig. 3). Circles and squares show the integrated contact intensities $I_{\mathrm{pair}}(a_s)$ and $I_k(a_s)$, respectively, determined from the pair distribution functions and the momentum distributions for $r_0 = 0.005a_{\mathrm{ho}}$ (see text for details). Panel (a) shows the entire crossover region on a logscale, while panels (b) and (c) show the negative and positive scattering length regions on a linear scale.

reflects the formation of pairs. The peak at smaller interparticle up-down distances r corresponds to the formation of a pair while the peak at larger r values ($r \approx 1a_{\mathrm{ho}}$ to $1.5a_{\mathrm{ho}}$) reflects the fact that the second up-atom and the second down-atom are pushed away from the first pair due to the Pauli exclusion principle (i.e., the formation
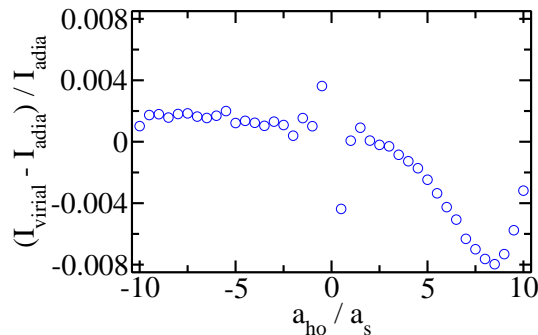
FIG. 3: (Color online) Fractional difference $[I_{\text{virial}}(a_s) - I_{\text{adia}}(a_s)]/I_{\text{adia}}(a_s)$ as a function of the inverse s-wave scattering length a_s^{-1}.

of self-bound trimers and tetramers is prohibited). (iii) The scaled pair distribution functions vanish at $r = 0$ for all s-wave scattering lengths; for numerical reasons, the first point of $P_{\text{pair}}(r)$ is not calculated at $r = 0$ but at $r = 0.005a_{\text{ho}}$. The vanishing of $P_{\text{pair}}(r)r^2$ at $r = 0$ is accompanied by a sharp drop of $P_{\text{pair}}(r)r^2$ at r values of the order of a few times the range r_0. The scaled pair distribution functions behave universally when r is larger than a few times the range r_0; for smaller r, the pair distribution functions acquire non-universal behavior.

To illustrate the universal, range independent behavior of the scaled pair distribution functions, Fig. 5 shows the quantity $(4\pi)^2 P_{\text{pair}}(r)r^2$ for a number of different r_0 but fixed s-wave scattering length, i.e., for $a_{\text{ho}}/a_s = -10$ (corresponding to $a_s = -0.1a_{\text{ho}}$). For this scattering length, the condition $r_0 \ll |a_s|$ is approximately fullfilled if $r_0 \lesssim 0.02a_{\text{ho}}$. In agreement with this condition, the universal part of the pair distribution functions $P_{\text{pair}}(r)$, i.e., the part where $P_{\text{pair}}(r)$ is independent of r_0, extends to smaller r values with decreasing r_0. Figure 5 shows that the scaled pair distribution functions for small r_0, $r_0 \lesssim 0.02a_{\text{ho}}$, behave approximately linearly in the regime $3r_0 \lesssim r \lesssim 0.05 - 0.1a_{\text{ho}}$; in this regime, essentially no dependence on r_0 is visible. The behavior of $P_{\text{pair}}(r)r^2$, illustrated exemplarily for $a_s = -0.1a_{\text{ho}}$ in Fig. 5, suggests that the integrated contact intensity $I_{\text{pair}}(a_s)$ can be determined readily by employing a linear two parameter fit to the small r-regime where the universal part of $(4\pi)^2 P_{\text{pair}}(r)r^2$ varies linearly and where $P_{\text{pair}}(r)$ is calculated for a finite but sufficiently small r_0. Alternatively, one might consider extrapolating the pair distribution functions themselves to $r_0 = 0$; this approach is not pursued in this work.

Figures 6(a)-6(c) illustrate our determination of $I_{\text{pair}}(a_s)$ for $a_{\text{ho}}/a_s = -5$, 0 and 5. We find that $I_{\text{pair}}(a_s)$, which is determined by the $r = 0$ value of the fit (i.e., the intercept), can be determined most reliably for large $|a_s|$ where the universal part of $P_{\text{pair}}(r)r^2$
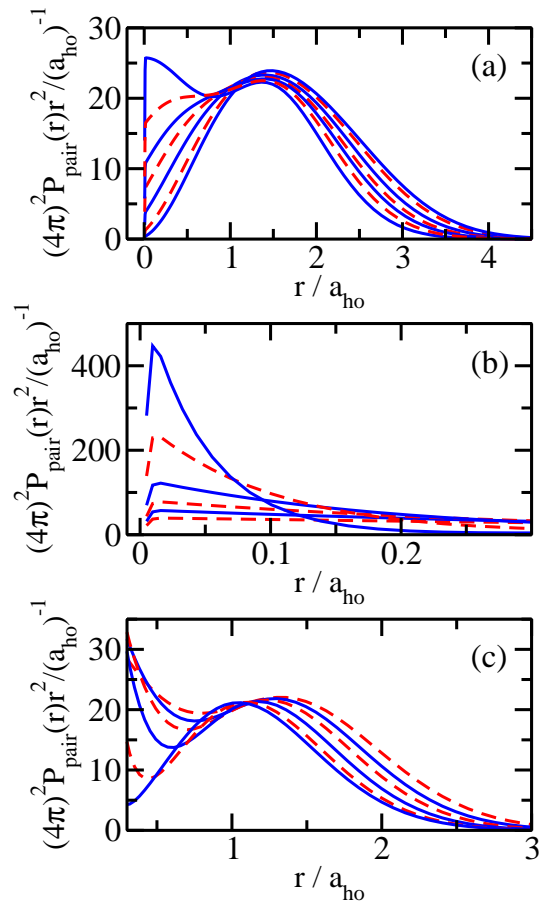

FIG. 4: (Color online) Scaled pair distribution functions $(4\pi)^2 P_{\text{pair}}(r)r^2$ as a function of r for $r_0 = 0.005a_{\text{ho}}$. Panel (a) shows the scaled pair distribution functions for $a_{\text{ho}}/a_s = -10$, -5, -2.5, -1.5, -1, -0.5 and 0 (from bottom to top at $r = 0.25a_{\text{ho}}$). Panels (b) and (c) show the scaled pair distribution functions for $r \leq 0.3a_{\text{ho}}$ and $r \geq 0.3a_{\text{ho}}$, respectively, for $a_{\text{ho}}/a_s = 0.5$, 1, 1.5, 2.5, 5 and 10 [from (b) bottom to top at $r = 0.05a_{\text{ho}}$ and (c) top to bottom at $r = 2a_{\text{ho}}$]. Note the different scales of the axes in panels (a) through (c).

that varies linearly extends over a comparatively large r range and where the slope is comparatively shallow. For small $|a_s|$, the extrapolated integrated contact intensity $I_{\text{pair}}(a_s)$ shows a notable dependence on the fitting range employed. The integrated contact intensity $I_{\text{pair}}(a_s)$, determined from the pair distribution functions for $r_0 = 0.005a_{\text{ho}}$, is shown by circles in Fig. 2. While $I_{\text{pair}}(a_s)$ compares very favorably with $I_{\text{adia}}(a_s)$ and $I_{\text{virial}}(a_s)$ in the strongly-interacting regime, $I_{\text{pair}}(a_s)$ is notably smaller than $I_{\text{adia}}(a_s)$ and $I_{\text{virial}}(a_s)$ in the weakly-attractive and weakly-repulsive regimes. It is clear from Figs. 6(a) through 6(c) that $I_{\text{pair}}(a_s)$ would be somewhat larger in the weakly-interacting regimes if the upper fitting limit was reduced somewhat (see also
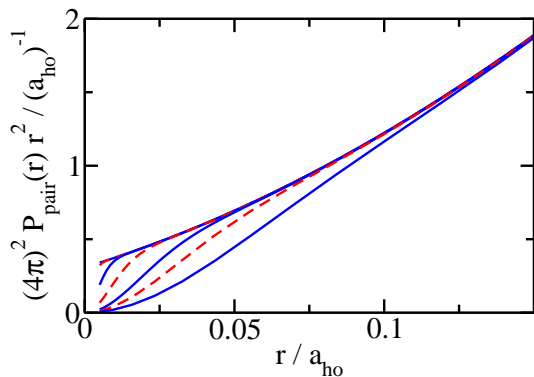
FIG. 5: (Color online) Scaled pair distribution functions $(4\pi)^2 P_{\mathrm{pair}}(r)r^2$ as a function of r, $r \in [0, 0.15a_{\mathrm{ho}}]$, for $a_{\mathrm{ho}}/a_s = -10$ and various r_0. At small r, the scaled pair distribution functions correspond from bottom to top to $r_0 = 0.05, 0.03, 0.02, 0.01, 0.005, 0.0025$, and $0.001a_{\mathrm{ho}}$. Note that the solid and dashed lines for the two smallest ranges, i.e., for $r_0 = 0.001$ and $0.0025a_{\mathrm{ho}}$, are nearly indistinguishable on the scale shown.

the caption of Fig. 6). This would bring $I_{\mathrm{pair}}(a_s)$ into even better agreement with $I_{\mathrm{adia}}(a_s)$ and $I_{\mathrm{virial}}(a_s)$ in the weakly-interacting regimes while leaving the behavior in the strongly-interacting regime essentially unchanged.

Figures 7(a) and 7(b) show the lowest partial wave projection $n_{00}(k)$ of the momentum distribution for fixed r_0, i.e., for $r_0 = 0.005a_{\mathrm{ho}}$, and selected negative and positive scattering lengths. For weak attraction, the lowest partial wave projection $n_{00}(k)$ is approximately Gaussian. As a_s^{-1} increases, $n_{00}(k)$ develops a tail at large k while the small k amplitude decreases. The tail at large k indicates that the system is characterized by increasingly small length scales, reflecting the formation of pairs.

To determine the integrated contact intensity $I_k(a_s)$ from the lowest partial wave projection $n_{00}(k)$, we scale $n_{00}(k)$ by k^4 and plot the resulting quantity as a function of k^{-1} [see Eq. (9) and Figs. 8(a) and 8(b)]. Similarly to our analysis of the scaled pair distribution functions, we extract the integrated contact intensity $I_k(a_s)$ by employing a linear two-parameter fit to the linear small k^{-1} region of $2\pi^2 4\pi n_{00}(k)/\sqrt{4\pi}$, where $n_{00}(k)$ is calculated for a small but finite r_0. Figures 8(a) and 8(b) illustrate the procedure for $a_{\mathrm{ho}}/a_s = -5$ and 0, respectively. The resulting integrated contact intensities $I_k(a_s)$, determined from the momentum distributions for $r_0 = 0.005a_{\mathrm{ho}}$, are shown as a function of the inverse s-wave scattering length a_s^{-1} by squares in Fig. 2. The agreement between $I_k(a_s)$ and the integrated contact intensities determined based on definitions (i) and (ii) is very good for $a_s^{-1} \lesssim 5$. For larger inverse scattering lengths, notable deviations are visible. These deviations can, as in the case of $I_{\mathrm{pair}}(a_s)$, be traced back to the fitting range
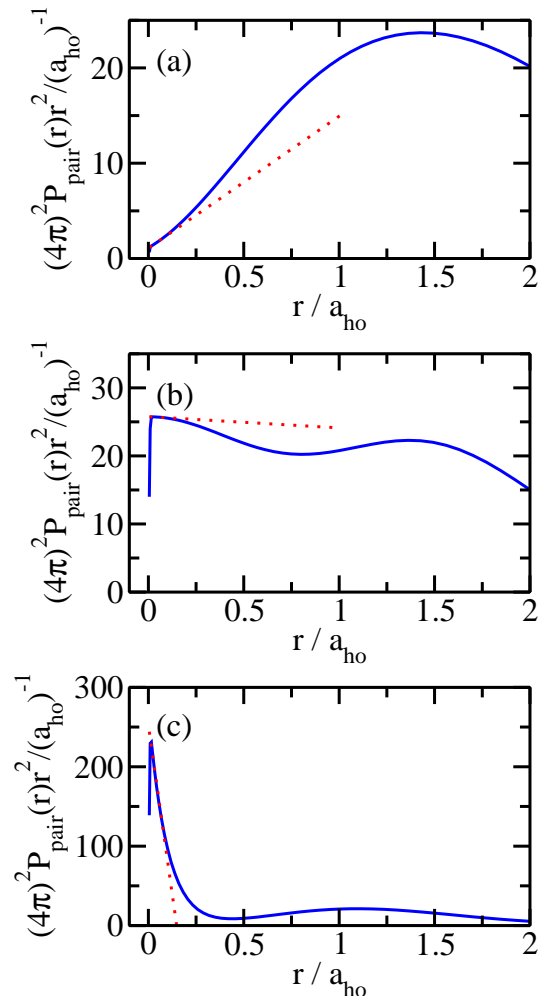

FIG. 6: (Color online) Solid lines show the scaled pair distribution functions $(4\pi)^2 P_{\mathrm{pair}}(r)r^2$ as a function of r for $r_0 = 0.005a_{\mathrm{ho}}$ and (a) $a_{\mathrm{ho}}/a_s = -5$, (b) $a_{\mathrm{ho}}/a_s = 0$ and (c) $a_{\mathrm{ho}}/a_s = 5$. The dotted lines are obtained by performing a linear two-parameter fit to the small r-region of the scaled pair distribution functions; the fit includes r-values in the range $[0.015a_{\mathrm{ho}}, 0.1a_{\mathrm{ho}}]$.

employed to extract $I_k(a_s)$. Despite these deviations, Figs. 2(a)-2(c) convincingly illustrate the equivalence of definitions (i) through (iv) of the integrated contact intensity.

IV. GENERALIZED VIRIAL THEOREM

Our total energies $E(a_s, r_0)$ and trap energies $V_{\mathrm{tr}}(a_s, r_0)$ for the energetically lowest-lying gas-like state of the four-fermion system can be readily combined to verify the generalized virial theorem derived by
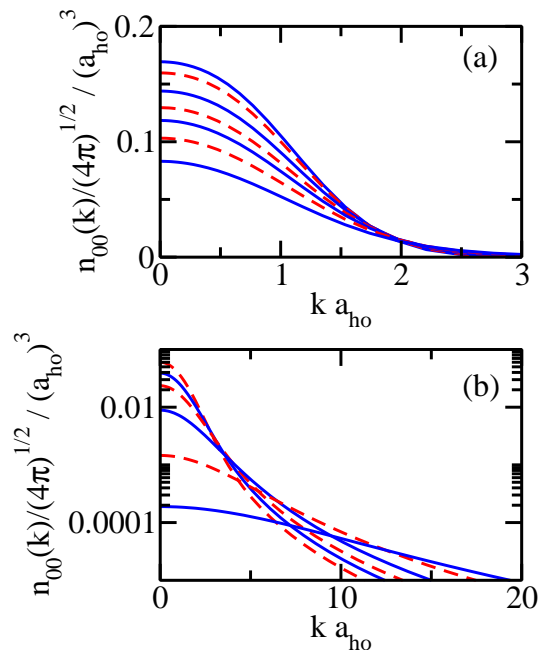
FIG. 7: (Color online) Scaled projected momentum distri bution $n_{00}(k)/\sqrt{4\pi}$ as a function of k for $r_0 = 0.005a_{\rm ho}$ Panel (a) shows the scaled projected momentum distributions for $a_{\rm ho}/a_s = -10, -5, -2.5, -1.5, -1, -0.5$ and 0 (from top to bottom at $k = 0.5a_{\rm ho}^{-1}$). Panel (b) shows the scaled projected momentum distributions for $a_{\rm ho}/a_s = 0.5, 1, 1.5, 2.5, 5$ and 10 (from top to bottom at $k = 1a_{\rm ho}^{-1}$). Note the different axes in panels (a) and (b).

FIG. 8: (Color online) The solid lines show the scaled projected momentum distribution $2\pi^2\, 4\pi\, n_{00}(k)/\sqrt{4\pi}$ as a function of k^{-1} for $r_0 = 0.005a_{\rm ho}$ and (a) $a_{\rm ho}/a_s = -5$ and (b) $a_{\rm ho}/a_s = 0$. The dotted lines are obtained by performing a linear two-parameter fit to the small k^{-1}-region of the scaled projected momentum distribution; the fit includes k^{-1}-values in the ranges (a) $[0.05a_{\rm ho}, 0.1a_{\rm ho}]$ and (b) $[0.03a_{\rm ho}, 0.1a_{\rm ho}]$.

Werner [17]. This theorem applies not only to infinitely large s-wave scattering lengths but also to finite scattering lengths and accounts for finite range corrections,

$$E(a_s, r_0) = 2V_{\rm tr}(a_s, r_0) - \frac{1}{2}a_s\frac{\partial E(a_s, r_0)}{\partial a_s} - \frac{1}{2}r_0\frac{\partial E(a_s, r_0)}{\partial r_0}. \quad (15)$$

Here, it is assumed that the underlying two-body potential $V_{\rm tb}$ depends on only two lengths, the s-wave scattering length a_s and the range r_0. The second term on the right hand side of Eq. (15) can be rewritten as $a_s^{-1}[\partial E(a_s, r_0)/\partial a_s^{-1}]/2$, which shows that it vanishes at unitarity. In the zero-range limit (i.e., for $r_0 = 0$), Eq. (15) thus reduces to the "usual" virial theorem $E(a_s, 0) = 2V_{\rm tr}(a_s, 0)$ [7, 8, 32, 33], which has been discussed in the context of Fig. 1(a).

Symbols in Fig. 9 show the fractional difference between the four-fermion energy $E_{\rm virial}(a_s, r_0)$ calculated according to the right hand side of Eq. (15) and the energy calculated by the CG approach as a function of the inverse scattering length a_s^{-1}. For negative scattering lengths, the virial theorem and CG energies agree to bet-
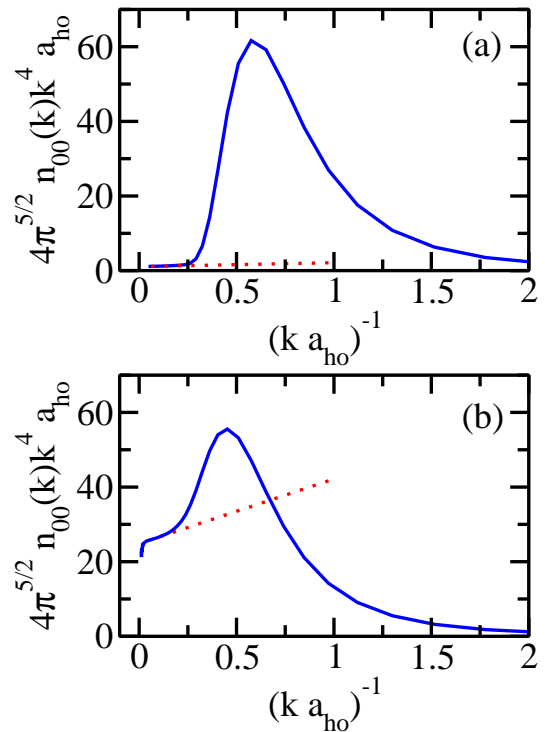
ter than 0.025% for the parameter combinations considered, thus confirming the generalized virial theorem with high accuracy. For positive scattering lengths, our results confirm the generalized virial theorem with 2% accuracy. We note that the validity of the generalized virial theorem has very recently also been investigated for large two-component Fermi gases by means of a Monte Carlo approach [35].

V. CONCLUSIONS

This paper investigates universal properties of dilute equal-mass two-component s-wave interacting Fermi gases. In particular, our calculations are performed for the energetically lowest-lying gas-like state of the trapped four-fermion system without spin-imbalance. We determined the energies and various other properties as functions of the scattering length and the range of the underlying two-body potential. Analyzing these quantities, we were able to explicitly demonstrate the equivalence of
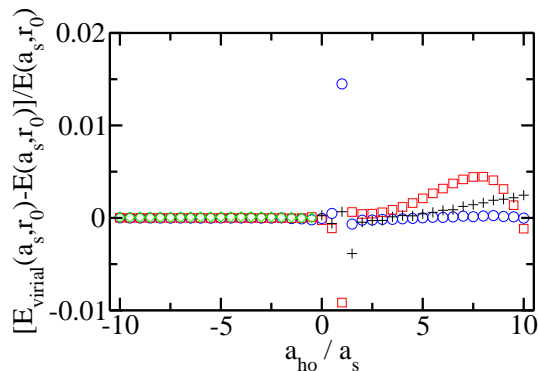
FIG. 9: (Color online) Fractional difference $[E_{\mathrm{virial}}(a_s, r_0) - E(a_s, r_0)]/E(a_s, r_0)$ as a function of the inverse s-wave scattering length a_s^{-1}. Pluses, circles, squares and diamonds show the fractional difference for $r_0 = 0.005, 0.01, 0.03$ and $0.05a_{\mathrm{ho}}$ (for negative a_s, only values for the largest three r_0 are shown; for positive a_s, only values for the smallest three r_0 are shown). For negative a_s, the absolute value of the fractional difference is smaller than 0.00025 for all r_0 shown.

four distinctly different definitions of the integrated contact intensity $I(a_s)$ [14, 15, 16] and of a generalized virial theorem [17] with high accuracy. In addition, we performed selected calculations for the energetically lowest-lying gas-like $L^\pi = 0^+$ state of the three-fermion system with $(N_\uparrow, N_\downarrow) = (2, 1)$ and the five-fermion system with $(N_\uparrow, N_\downarrow) = (3, 2)$. These calculations confirm our findings discussed in Sec. III for the four-fermion system. We

have outlined in detail how the integrated contact intensities $I_{\mathrm{pair}}(a_s)$ and $I_k(a_s)$ can be extracted from our numerical data. While we have not commented on how to best measure the integrated contact intensity experimentally, our outlined analysis provides some guidance as to the demands on the accuracy of experimental data if the integrated contact intensity is to be measured with high accuracy. At the same time, we have shown that the integrated contact intensity changes by multiple orders of magnitude through the crossover, making a qualitative measurement of $I(a_s)$ appear quite plausible.

The explicit verification of the universal relations away from unitarity paves the way for developing the concept of the integrated contact intensity further. For example, are there other properties of the many-body two-component Fermi gas besides those already discussed [14, 15, 16] that are related through the integrated contact intensity? Can the concept of the integrated contact intensity be extended to low-dimensional systems? Furthermore, can the concept of the integrated contact intensity be extended to relate various properties of unequal-mass two-component Fermi gases with large mass ratio or Bose gases? For these systems, a three-body parameter that is associated with Efimov physics [36, 37] arises and it has been speculated [18] that this three-body parameter could somehow be related to an integrated contact intensity that, physically speaking, accounts for the formation of trimers.

[1] G. A. Baker, Jr., Phys. Rev. C **60**, 054311 (1999).
[2] K. M. O'Hara, S. L. Hemmer, M. E. Gehm, S. R. Granade, and J. E. Thomas, Science **298**, 2179 (2002).
[3] T.-L. Ho, Phys. Rev. Lett. **92**, 090402 (2004).
[4] S. Y. Chang and V. R. Pandharipande, Phys. Rev. Lett. **95**, 080402 (2005).
[5] G. E. Astrakharchik, J. Boronat, J. D. Casulleras, and S. Giorgini, Phys. Rev. Lett. **93**, 200404 (2004).
[6] S. Y. Chang, V. R. Pandharipande, J. Carlson, and K. E. Schmidt, Phys. Rev. A **70**, 043602 (2004).
[7] J. E. Thomas, J. Kinast, and A. Turlapov, Phys. Rev. Lett. **95**, 120402 (2005).
[8] F. Werner and Y. Castin, Phys. Rev. A **74**, 053604 (2006).
[9] D. T. Son and M. Wingate, Ann. Phys. **321**, 197 (2006).
[10] S. Tan, cond-mat/0412764v2 (2004).
[11] T. Busch, B.-G. Englert, K. Rzążewski, and M. Wilkens, Foundations of Phys. **28**, 549 (1998).
[12] F. Werner and Y. Castin, Phys. Rev. Lett. **97**, 150401 (2006).
[13] D. Blume, J. von Stecher, and C. H. Greene, Phys. Rev. Lett. **99**, 233201 (2007).

[14] S. Tan, Ann. Phys. **323**, 2952 (2008).
[15] S. Tan, Ann. Phys. **323**, 2971 (2008).
[16] S. Tan, Ann. Phys. **323**, 2987 (2008).
[17] F. Werner, Phys. Rev. A **78**, 025601 (2008).
[18] E. Braaten and L. Platter, Phys. Rev. Lett. **100**, 205301 (2008).
[19] E. Braaten, D. Kang, and L. Platter, Phys. Rev. A **78**, 053606 (2008).
[20] S. Giorgini, L. P. Pitaevskii, and S. Stringari, Rev. Mod. Phys. **80**, 1215 (2008).
[21] M. Greiner, C. A. Regal, and D. S. Jin, Nature **426**, 537 (2003).
[22] M. W. Zwierlein, C. A. Stan, C. H. Schunck, S. M. F. Raupach, S. Gupta, Z. Hadzibabic, and W. Ketterle, Phys. Rev. Lett. **91**, 250401 (2003).
[23] T. Stöferle, H. Moritz, K. Günter, M. Köhl, and T. Esslinger, Phys. Rev. Lett. **96**, 030401 (2006).
[24] T. Köhler, K. Goral, and P. S. Julienne, Rev. Mod. Phys. **78**, 1311 (2000).
[25] E. Nielsen, D. V. Fedorov, A. S. Jensen, and E. Garrido, Phys. Rep. **347**, 374 (2001).
[26] Y. Suzuki and K. Varga, *Stochastic Variational Approach*

to Quantum Mechanical Few-Body Problems (Springer Verlag, Berlin, 1998).

[27] H. H. B. Sørensen, D. V. Fedorov, and A. S. Jensen, Nuclei and Mesoscopic Physics, ed. by V. Zelevinsky, AIP Conf. Proc. No. 777 (AIP, Melville, NY, 2005), p. 12.

[28] J. von Stecher and C. H. Greene, Phys. Rev. Lett. **99**, 090402 (2007).

[29] J. von Stecher, C. H. Greene, and D. Blume, Phys. Rev. A **77**, 043619 (2008).

[30] D. S. Petrov, Phys. Rev. A **67**, 010703(R) (2003).

[31] D. S. Petrov, C. Salomon, and G. V. Shlyapnikov, Phys. Rev. Lett. **93**, 090404 (2004).

[32] D. T. Son, arXiv:0707.1851v1 (2007).

[33] T. Mehen, arXiv:0712.0867v1 (2007).

[34] J. von Stecher and C. H. Greene, Phys. Rev. A **80**, 022504 (2009).

[35] L. E. C. Rosales-Zarate and R. Jauregui, arXiv:0909.0673 (2009).

[36] V. Efimov, Yad. Fiz. **12**, 1080 (1970) [Sov. J. Nucl. Phys. **12**, 598 (1971)].

[37] V. N. Efimov, Nucl. Phys. A **210**, 157 (1973).